

Does the A-type Metallic-line Star IW Persei Have Non-Uniform Chemical Anomaly on the Surface?

Y. T a k e d a

11-2 Enomachi, Naka-ku, Hiroshima-shi, Japan 730-0851
e-mail: ytakeda@js2.so-net.ne.jp

Received May 29, 2023

ABSTRACT

IW Per, a single-lined spectroscopic binary with a short period of 0.92 d, is known to be a A-type metallic-line (Am) star showing anomalous line strengths of specific elements. Previously, Kim (1980) reported that its equivalent widths of Ca II 3934, Sr II 4215, and Sc II 4320 lines (important key lines characterizing the Am anomaly) show cyclic variations in accordance with the rotation phase, implying that the chemical peculiarities on the surface are not uniform but of rather patchy distribution, though no trial of reconfirmation seems to have been done so far. In order to check the validity of this finding, 10 high-dispersion spectra of IW Per covering different phases were analyzed for these lines by using the spectrum-fitting technique to determine the abundances of Ca, Sr, and Sc and the corresponding equivalent widths. It turned out, however, that no firm evidence of such phase-dependent line-strength variations could be found, suggesting that significant chemical inhomogeneity on the surface of IW Per is unlikely to exist, at least as regards to the period of our observations (2010 December). Meanwhile, the abundances of O, Si, Ca, Ba, and Fe resulting from the 6130–6180 Å region corroborate that IW Per is a distinct Am star (though the degree of peculiarity differs from element to element) despite that its rotational velocity ($\sim 100 \text{ km s}^{-1}$) is near to the existent limit of Am phenomenon.

Key words: *stars: abundances – stars: chemically peculiar – stars: early-type – stars: individual (IW Per) – stars: spectroscopic binaries*

1. Introduction

IW Per is a spectroscopic binary of a short period (~ 0.92 d), where lines of only the primary mid A-type star is visible in the spectrum. It is also a photometric variable with small amplitudes of several hundredths mag, which is because of the aspect effect on an ellipsoidal stellar shape caused by the considerable centrifugal force due to rapid rotation (ellipsoidal variable). About four decades ago, Kim (1980) carried out an intensive photometric and spectroscopic study of this single-lined binary system, and established the orbital elements and stellar physical parameters by analyzing the observed radial velocity curve as well as the light curve, as summarized in Table 1.

As an important feature from the viewpoint of spectral classification, this star belongs to the group of “A-type metallic-line (Am) stars”, which is a subclass of chemically peculiar (CP) stars (upper main-sequence stars showing unusual spectra). Am stars are known to have the following characteristics (see, e.g., Conti 1970 or Preston 1974).

- Metallic lines (such as Fe) are stronger while the Ca II 3934 line (K line) is weaker in comparison with normal stars, which are used (along with Balmer lines) for spectral classification of A-type stars. Accordingly, spectral types of Am stars estimated from different indicators are discordant with each other as $\text{Sp}(\text{Ca K}) < \text{Sp}(\text{Balmer}) < \text{Sp}(\text{metal})$.
- According to chemical abundance studies based on high-dispersion spectra, Ca and Sc (as well as light elements such as C, N, and O) are deficient while heavier elements (Fe group or s-process elements such as Sr or Ba) are overabundant in Am stars.
- Rotational velocities of Am stars are generally lower (typical $v_e \sin i$ is on the order of several tens km s^{-1}), despite that many ordinary A stars are rapid rotators (mean $\langle v_e \sin i \rangle$ is $\sim 100\text{--}200 \text{ km s}^{-1}$; e.g., Abt & Morrell 1995). As a matter of fact, no Am stars are ever found at $v_e \sin i \gtrsim 100 \text{ km s}^{-1}$.
- There is a trend that Am phenomenon appears especially in spectroscopic binaries. This high frequency of Am stars in close binaries may be related to the preference of slow rotational velocity mentioned above, because rotation tends to be decelerated by tidal braking.

Interestingly, Kim (1980) found from his spectrograms (used for measuring radial velocities) that the strengths of Am-specific lines in IW Per show appreciable cyclic variations (by $\sim 10\text{--}20\%$) with the rotation phase: that is, the equivalent widths of Ca II 3934 as well as Sc II 4320 lines reach the weak bottom around phases of ~ 0.25 and ~ 0.75 , where that of Sr II 4215 line conversely attains the strong peak (cf. Fig. 8 of Kim 1980). This implies that the chemical anomaly is not uniform over the surface of IW Per but has rather inhomogeneous or patchy distribution.

This is a noteworthy result, because very few Am stars are known to exhibit such a phase-dependent line-strength variability, although aspect-dependent spectrum variations due to patchy distribution of specific elements are actually observed in other class of CP stars (e.g., magnetic stars of SrEuCr type). Is IW Per the first Am star with inhomogeneous chemical distribution on the surface?

However, very little attention seems to have been paid to this finding so far, unfortunately. Considering that Kim’s result was based on photographic spectrograms, which are outdated from the viewpoint of present-day standard, it needs to be reconfirmed by all means.

Accordingly, the author decided to check whether the strengths of Ca II 3934, Sr II 4215, and Sc II 4320 lines in IW Per show such significant phase-dependent variations as found by Kim (1980), while using new observational materials (10 CCD spectra reasonably covering the phases) and efficient analysis techniques (spectrum-fitting analysis). This is the primary purpose of the investigation. In connection with this inspection, since IW Per is an ellipsoidal variable with inhomogeneous distribution of T (temperature) and g (surface gravity) on the distorted surface, the impact of this effect on spectrum variation is also estimated based on the Roche model.

Besides, the quantitative nature of Am anomaly in IW Per is examined by determining the abundances of key elements (O, Si, Ca, Ba, and Fe) and comparing them with those of many A-type stars, which is counted as another aim of the present investigation. This is worthwhile because IW Per is a rapid rotator ($v_e \sim 100 \text{ km s}^{-1}$) almost near to the existent limit of Am phenomenon,

2. Observational data

The observations of IW Per were carried out on 2010 December 14, 15, 16, 18, and 20 by using BOES (Bohyunsan Observatory Echelle Spectrograph) attached to the 1.8 m reflector at Bohyunsan Optical Astronomy Observatory in the Republic of Korea. Using $2k \times 4k$ CCD (pixel size of $15 \mu\text{m} \times 15 \mu\text{m}$), this echelle spectrograph enabled us to obtain spectra of wide wavelength coverage (from $\sim 3800 \text{ \AA}$ to $\sim 9200 \text{ \AA}$) with the resolving power of $R \simeq 45000$ (use of $200 \mu\text{m}$ fiber). The observations were done 1–3 times in a night with an interval of a few hours. Thus, as a result of 5-night observations, 10 spectra were obtained in total (each consisting of 1 or 2 successive frames of 15–20 min exposure to be co-added). The total integration time for each spectrum was 15–40 min. The fundamental information (spectrum code, observed time in Julian day, mean S/N ratios around the relevant regions, etc.) for each of the 10 spectra is presented in Table 2.

The reduction of the echelle spectra (bias subtraction, flat fielding, spectrum extraction, wavelength calibration, and continuum normalization) was carried out by using the software package IRAF (Image Reduction and Analysis Facility).¹

The orbital phase corresponding to the observed time (at the mid exposure) of each spectrum was calculated by the ephemeris

$$\text{Minimum} = \text{JD}2433617.317 + 0.9171877E \quad (E : \text{integer}) \quad (1)$$

which was taken from Eq.(2) of Kim (1980). The observed heliocentric radial velocities (V_r^{hel}) were determined from the spectrum fitting in the 6130–6180 \AA region (cf. Sect. 4), which are also given in Table 2. The resulting V_r^{hel} values are

¹IRAF is distributed by the National Optical Astronomy Observatories, which is operated by the Association of Universities for Research in Astronomy, Inc. under cooperative agreement with the National Science Foundation.

plotted against the phase in Fig. 1, where the velocity results derived by Kim (1980) are also overplotted for comparison. As seen from this figure, both are reasonably consistent with each other.

3. Standard model atmosphere

As mentioned in Sect. 1, IW Per is an ellipsoidal variable, in which physical conditions on the surface are not uniform, and thus can not be described in the strict sense by only one model atmosphere. Still, it is meaningful to define the “standard” model atmosphere well representing the averaged physical properties of this star, which is to be used for the analysis of the spectra in Sect. 4.

The atmospheric parameters for this standard model were established in the same manner as done in Takeda et al. (2008, 2009). The effective temperature (T_{eff}) and surface gravity ($\log g$) were evaluated from the colors of Strömgren’s $uvby\beta$ photometric system with the help of the UVBYBETANEW program (Napiwotzki et al. 1993). The observed $uvby\beta$ data for IW Per were taken from Paunzen’s (2015) compilation. Since these colors fit in two processing groups (groups 5 and 6) of the UVBYBETANEW program, both groups were attempted, from which ($T_{\text{eff}}, \log g$) of (8439 K, 4.21) and (8303 K, 4.22) were derived for group 5 and group 6, respectively. Consequently, the simple mean of these two results (8371 K, 4.22) were adopted.

Regarding the microturbulence (v_t), Takeda et al.’s (2008) empirical relation (reasonably representing the observed trend of v_t with uncertainties of $\pm 30\%$)

$$v_t = 4.0 \exp\{-[\log(T_{\text{eff}}/8000)/A]^2\} \quad (2)$$

(where $A \equiv [\log(10000/8000)]/\sqrt{\ln 2}$) was adopted, which gives $v_t = 3.89 \text{ km s}^{-1}$ for $T_{\text{eff}} = 8371 \text{ K}$.

The adopted color data along with the resulting values of T_{eff} , $\log g$, and v_t are also summarized in Table 1. The model atmosphere was then constructed by two-dimensionally interpolating Kurucz’s (1993) ATLAS9 model grid in terms of T_{eff} and $\log g$, where the solar-metallicity models were employed.

4. Spectrum fitting analysis

The procedures for deriving the abundances and equivalent widths are the same as adopted in previous papers (e.g., Takeda et al. 2008, 2009), which are based on the spectrum fitting program MPFIT developed by Takeda (1995). This program establish the solutions for (i) the abundances of relevant elements (A_1, A_2, \dots), (ii) projected rotational velocity ($v_e \sin i$), and (iii) radial velocity (V_r) by accomplishing the best fit (minimizing $O - C$ residuals) between theoretical and observed spectra.

This fitting analysis was applied to the following four regions in this study.

- 3925–3942 Å region (Ca and Fe abundances varied)
The aim is to evaluate the equivalent width of Ca II 3934 line from the resulting Ca abundance.
- 4207–4224 Å region (Sr and Fe abundances varied)
The aim is to evaluate the equivalent width of Sr II 4215 line from the resulting Sr abundance.
- 4316.5–4327.5 Å region (Sc, Ti, and Fe abundances varied)
The aim is to evaluate the equivalent width of Sc II 4320 line from the resulting Sc abundance.
- 6130–6180 Å region (O, Si, Ca, Ba, and Fe abundances varied)
The aim is to determine the abundances of O, Si, Ca, Ba, and Fe (along with $v_e \sin i$ and V_r)

The abundances of all other elements (except for those varied) were fixed at the solar abundances during the iterative fitting procedure.

The assumption of LTE (Local Thermodynamic Equilibrium) was applied to theoretical calculations of all lines in this study. The atomic data of the spectral lines were adopted from Kurucz & Bell's (1995) compilation, except for those of 3925–3942 Å region which were taken from the VALD database (Ryabchikova et al. 2015). In case that data of damping parameters are not available, the default treatment of the WIDTH9 program (Kurucz 1993) was employed. The λ , χ_{low} , and gf values of selected important lines are summarized in Table 3. Figs. 2–5 display how the theoretical spectra for the converged solutions fit well with the observed spectra for each region.

Then, after the abundances (A) have been established, the equivalent widths of Ca II 3934, Sr II 4215, and Sc II 4320 lines (W_{3934} , W_{4215} , and W_{4320}) were calculated inversely from $A(\text{Ca})$, $A(\text{Sr})$, and $A(\text{Sc})$ with the help of Kurucz's (1993) WIDTH9 program. The final results are summarized in Table 4. In Figs. 2–5 are also plotted the resulting A as well as W against the corresponding phase.

5. Model star simulation

Before discussing the behaviors of Ca II, Sr II, and Sc II lines with the phase, it is meaningful to check how the aspect change to this ellipsoidal variable (where surface physical parameters are position-dependent) potentially affects the observed quantities. For this purpose, the surface structure of the primary star was simulated based on the Roche model. By using the masses (M_1 , M_2) and the distances to the gravity center (a_1 , a_2) determined by Kim (1980; cf. Table 1), the shape of the primary $r(\theta, \phi)$ can be calculated from the equi-potential surface with the boundary condition of $r(\theta = 0^\circ) = 1.7R_\odot$ ($\equiv R_p$: polar radius), and the distribution of local surface gravity $g(\theta, \phi)$ ($\equiv |\mathbf{g}_1 + \mathbf{g}_2 + \mathbf{g}_{\text{cf}}|$) is also derived, where \mathbf{g}_1 , \mathbf{g}_2 , and \mathbf{g}_{cf}

are the gravity force from M_1 , gravity force from M_2 , and the centrifugal force, respectively. Further, assuming $T_{\text{eff,p}} = 8500 \text{ K}$ (polar T_{eff} at $\theta = 0^\circ$) and applying the relation of $T_{\text{eff}} \propto g^{1/4}$ (von Zeipel's law, which holds for the present case of $T_{\text{eff}} \gtrsim 8000 \text{ K}$), T_{eff} is expressed as a function of (θ, ϕ) . The resulting distributions of r , g , and T_{eff} are illustrated in Figs. 6a–6c. Comparing these results with those obtained by Kim (1980; cf. Sect. 6 in his paper), we can confirm a reasonable consistency with each other.

This distorted rotating star is viewed by an observer with the inclination angle (angle between the rotational axis and the line of sight) of $i = 63^\circ$, and the appearance as well as the properties of the visible disk change with the rotational phase (cf. Fig. 7a). Here, we define D (disk area), $\langle T_{\text{eff}} \rangle$ (mean T_{eff} averaged over the disk; in K), $\langle \log g \rangle$ (mean $\log g$ averaged over the disk; in dex), F_{5550} (observed monochromatic flux by the earth's observer at the representative V -band wavelength of 5550 \AA ; in $\text{erg s}^{-1} \text{cm}^{-2} \text{\AA}^{-1}$) as follows.

$$D \equiv \iint_{\text{disk}} d\xi d\eta, \quad (3)$$

$$\langle \log g \rangle \equiv \iint_{\text{disk}} \log g(\xi, \eta) I_{5550}(\xi, \eta) d\xi d\eta / \iint_{\text{disk}} I_{5550}(\xi, \eta) d\xi d\eta, \quad (4)$$

$$\langle T_{\text{eff}} \rangle \equiv \iint_{\text{disk}} T_{\text{eff}}(\xi, \eta) I_{5550}(\xi, \eta) d\xi d\eta / \iint_{\text{disk}} I_{5550}(\xi, \eta) d\xi d\eta, \quad (5)$$

and

$$F_{5550} \equiv \iint_{\text{disk}} I_{5550}(\xi, \eta) d\xi d\eta / d^2, \quad (6)$$

where $I_{5550}(\xi, \eta)$ is the specific intensity at 5550 \AA emergent from a point on the disk (ξ, η) toward the direction of the observer, and d ($= 56.47 \text{ pc} = 1.742 \times 10^{20} \text{ cm}$) is the distance to IW Per (Gaia DR2 parallax is 17.71 milliarcsec). I_{5550} at each point of the stellar disk was evaluated by interpolating the specific intensity grid $I_\lambda(\mu, T_{\text{eff}}, \log g)$ (μ is the direction cosine) of ATLAS solar metallicity models, which was downloaded from the Kurucz site² (filename: ip00k2.pck19). The runs of D , $\langle \log g \rangle$, $\langle T_{\text{eff}} \rangle$, and F_{5550} with the rotation phase are depicted in Figs. 7b–7e.

In Fig 7e, the observed flux of $-0.4V - 8.403$ (V is the V -band magnitude of IW Per taken from Kim 1980) is also plotted against the phase. Here, the constant of -8.403 was so chosen (by eye inspection) as to accomplish a match with $\log F_{5550}$. Since the absolute calibration relation between F_{5556} ($\text{erg cm}^{-2} \text{s}^{-1} \text{\AA}^{-1}$) and V (mag) gives -8.449 for this constant according to Eq.(10.4) of Gray (2005), the difference between these two makes $(-8.403) - (-8.449) = 0.046 \text{ dex}$, which may be further reduced down to $0.046 - 0.032 = 0.014 \text{ dex}$ by subtracting 0.032 ($= 0.4 \times 0.08$) dex due to the interstellar extinction effect of $A_V = 0.08(\pm 0.23) \text{ mag}$ (estimated by the EXTINCT program of Hakkila et al. 1997). This consistency in

²<http://kurucz.harvard.edu/grids/gridp00/>

the offset constant indicates that our model reproduces the observed energy distribution of IW Per satisfactorily (not only the relative change with the phase but also in terms of the absolute scale).³

6. Search for spectrum variability

6.1. Comparison with Kim's (1980) equivalent widths

We are now ready to discuss whether IW Per shows any variability in the strengths of specific lines characterizing the Am anomaly (Ca II 3934, Sr II 4215, and Sc II 4320) as reported by Kim (1980). Several characteristic trends can be seen from Figs. 2c, 3c, and 4c, where his W vs. phase relations (solid lines) with those derived in this study (symbols) are compared.

Kim's (1980) W values tend to be systematically larger especially for W_{4215} (by ~ 0.1 – 0.2 dex) and W_{4320} (~ 0.1 dex), which is likely to be related to the adopted procedure of W evaluation. Kim (1980) measured W directly from the spectrum with respect to the empirically placed continuum level. Though this is a conventional approach, uncertainties are inevitable because target lines are by no means isolated but more or less blended with other lines especially in the crowded blue region. In contrast, the equivalent width derived in this study represents only the pure contribution of the line in question, because it was calculated from the abundance of the relevant element resulting from the spectrum fitting analysis. It is thus understandable that such a methodological difference may have caused an appreciable discrepancy in the absolute values of W .

Therefore, we focus on the nature of “relative variation” in $\log W$. Are the phase-dependent strength variations of Am-specific lines reported by Kim (1980) (i.e., Am anomalies are enhanced around phases of $\sim 0.25/0.75$ while weakened around $\sim 0.0/0.5$) confirmed also in our observational data?

— Interestingly, somewhat similar trend may be seen for the Ca II 3934 line, since it appears to show a weak variation of W_{4215} with a minimum at phase of ~ 0.8 (Fig. 2c) like the case of Kim (1980).

— However, regarding the other two lines (Sr II 4215 and Sc II 4320), we do not see any signature of meaningful cyclic variation in their strengths (Figs. 3c and 4c) unlike his measurements.

— Especially, only small fluctuation of W_{4215} by a few percent ($\pm \lesssim 0.02$ dex) seriously conflicts Kim's (1980) result not only in terms of its size (the change he found amounts to $\sim \pm 0.05$ dex) but also in the sense of variation (our W_{4215} shows a minimum around phase ~ 0.2 where his W_{4215} has a maximum).

³It should be noted, however, that F_{5550} was calculated based on the disk-integration of the model star for the primary, while neglecting the contribution from the secondary, which Kim (1980) presumed to be a G0 V star from its mass of $1.08M_{\odot}$. Therefore, this consistency in the absolute sense should not be taken too seriously, as it might be something like fortuitous.

— Accordingly, it is reasonable to state that our observational data could not confirm the previous results of Kim (1980).

6.2. Origin of line strengths fluctuations

Here, it is worth discussing the cause of fluctuations in our W ($\pm\sigma_W/\langle W \rangle$), which are $\sim \pm 0.05$, $\sim \pm 0.04$, and $\sim \pm 0.03$ according to Table 4 for Ca II 3934, Sr II 4215, and Sc II 4320, respectively (or $\sim \pm 0.02$ dex, $\sim \pm 0.017$ dex, and $\sim \pm 0.01$ dex in $\log W$).

First, measurement errors involved in our W values should be examined. Here, the most important factor is the uncertainty in the continuum level.⁴ The spectrum-fitting method (Takeda 1995) adopted in Sect. 4 does not require any empirical specification of the continuum position (F_c) in advance; but F_c is theoretically determined after the fitting has been established. Any kind of spectrum change (e.g., due to noise) would cause an ambiguity in F_c . The equivalent width is approximately expressed as $W \simeq H(1 - F_0/F_c)$, where F_0 is the line-center flux and H is the full-width at half-maximum of the line. If the continuum level is perturbed as $F'_c = F_c(1 + \varepsilon)$ (where ε is the relative error in F_c ; $|\varepsilon| \ll 1$) and H as well as F_0 are assumed to be unchanged, then the ratio of the corresponding equivalent widths (W' and W) can be written as

$$W'/W \simeq 1 + \varepsilon(F_0/F_c)/(1 - F_0/F_c). \quad (7)$$

Since this relation suggests $W'/W \sim 1 + \varepsilon/(1 - F_0/F_c)$ at the weak-line limit ($F_0/F_c \lesssim 1$) and $W'/W \simeq 1 + \varepsilon(F_0/F_c) (\simeq 1)$ (i.e., practically ε -independent) at the strong-line limit ($F_0/F_c \simeq 0$), the effect of ε on W'/W becomes progressively important as the line gets weaker. Let us tentatively set $\varepsilon (\sim (S/N)^{-1}) = \pm 0.01$ (for Ca II 3934) and ± 0.005 (for Sr II 4215 and Sc II 4320) based on the typical S/N ratios given in Table 2. Considering that the relevant F_0/F_c values are ~ 0.2 , ~ 0.85 , and ~ 0.9 (relative to the local H γ wing) for Ca II 3934, Sr II 4215, and Sc II 4230, the resulting changes of $\log(W'/W)$ are ± 0.001 dex, ± 0.01 dex, and ± 0.02 dex, respectively.

Next, we estimate the effects due to the modulation of mean atmospheric parameters, which are $\sim \pm 0.005$ dex in $\langle \log g \rangle$ (Fig. 7c) and $\sim \pm 20$ K in $\langle T_{\text{eff}} \rangle$ (Fig. 7d). According to the parameter sensitivity of W_{3934} , W_{4215} , and W_{4320} shown in Table 5, the former $\log g$ effect is essentially negligible (< 0.001 dex in any case), while the latter T_{eff} effect (relative change in W for ± 20 K) is ± 0.018 , ± 0.006 , and ± 0.008 (or ± 0.0077 dex, ± 0.0026 dex, and ± 0.0035 dex in $\log W$). It is worth keeping in mind that the Ca II 3934 line is more sensitive to this $\langle T_{\text{eff}} \rangle$ modulation (by a factor of ~ 2 – 3) than the other 2 lines.

⁴Errors in W due to pure photometric origin (δW) were also estimated by using Cayrel's (1988) formula (depending on S/N, pixel size, and line widths) but turned out insignificant: $\delta W_{3934} \sim 2$ – 5 mÅ (~ 10 mÅ only for 1220C), $\delta W_{4215} \sim 1$ – 3 mÅ and $\delta W_{4320} \sim 1$ – 2 mÅ.

Based on these two rough considerations, it may be possible to explain (at least qualitatively) the cause of observed fluctuations (by $\sim \pm 0.01$ – 0.02 dex) in our $\log W_{3934}$, $\log W_{4215}$, and $\log W_{4320}$.

— Regarding the strong Ca II 3934 line, while the effect of continuum uncertainty is inessential, the cyclic change of $\langle T_{\text{eff}} \rangle$ by ± 20 K may cause a variation of $\sim \pm 0.01$ dex in $\log W_{3934}$. That the minimum of W_{3934} is observed around phase ~ 0.8 (cf. Fig. 2c) is consistent with this interpretation, because $\langle T_{\text{eff}} \rangle$ attains a maximum (making W_{3934} weaker) around this phase.

— In contrast, as to the weaker Sr II 4215 and Sc II 4230 lines, even slight uncertainties (by \pm several tenths percent) in the continuum position would result in appreciable changes by $\sim \pm 0.01$ – 0.02 dex in $\log W_{4215}$ as well as $\log W_{4320}$, to which the observed fluctuations may be attributed.

6.3. Absence of non-uniform surface chemical anomaly

As described in Sect. 6.1, our W_{3934} , W_{4215} , and W_{4320} values do not show clear cyclic variations, contrary to Kim's (1980) finding. It was also shown in Sect. 6.2 that the extents of their fluctuations may be understood in terms of possible errors in W due to continuum uncertainty (plus the effect of slight change in $\langle T_{\text{eff}} \rangle$ for Ca II 3934). Therefore, as far as our observational data are concerned, we do not see any evidence for an inhomogeneous distribution of Am anomaly on the surface of IW Per suspected by Kim (1980).

Also, this consequence is corroborated by the spectrum-fitting analysis of the 6130–6180 Å region (Fig. 5a), which yielded the abundances of O, Si, Ca, Ba, and Fe. Since lines are less crowded in this orange region as compared with the blue–violet region, the resulting abundances are considered to be more reliable. As seen from Figs. 5b–5f, no clear phase-dependence is observed in the resulting abundances showing only small dispersions (σ_A is ~ 0.01 – 0.02 dex for O, Ca, Fe; ~ 0.04 dex for Si and Ba; cf. Table 4). Moreover, we do not see any distinct interrelation between these abundances. This may be counted as another counterexample, because such an inhomogeneous distribution of Am peculiarity (if any exists) would reveal some kind of anticorrelation between the deficiency group (O, Ca) and enrichment group (Si, Ba, Fe).

Although our conclusion is in conflict with that of Kim (1980), this does not necessarily mean that his result was incorrect. What we can state is that non-uniform Am anomaly on the surface of IW Per is unlikely at the time of our observations (2010 December). We can not rule out a possibility that the nature of Am phenomenon changes in the course of time and it might have been actually patchy at the period of Kim's (1980) spectroscopic observations (1976–1977). Generally speaking, however, Kim's (1980) results had better be viewed with caution because his equivalent widths were measured on photographic spectrograms of insufficient quality.

7. Status of IW Per as an Am star

Another significant topic related to IW Per is its degree of Am peculiarity. Since synchronization is considered to be achieved in this short-period close binary system, the equatorial rotational velocity of the primary is expected as $v_e = (2\pi \times 1.05R_p)/P = 99 \text{ km s}^{-1}$, which is in agreement with the value of $v_e = 98 \text{ km s}^{-1}$ derived from the observed $v_e \sin i$ ($= 87 \text{ km s}^{-1}$; Table 4) and known i ($= 63^\circ$; Table 1). Therefore, IW Per is characterized by its high rotational velocity ($v_e \simeq 100 \text{ km s}^{-1}$) for an Am star, which is near to the upper limit for the appearance of Am phenomenon ($v_e \sin i \lesssim 100 \text{ km s}^{-1}$; cf. Sect. 1).

In view of the fact that Am stars are found only in this comparatively lower $v_e \sin i$ range, it has been a controversial issue whether the degree of anomaly progressively fades away with an increase of $v_e \sin i$ (e.g., Kodaira 1975; Takeda & Sadakane 1997) or Am peculiarity tends to persist without such a systematic change up to the limit (e.g., Burkhart 1979). It is thus meaningful to examine the nature and extent of chemical anomaly in this rare rapidly-rotating Am star by comparing with other normal A and Am stars of various rotational velocities.

Conveniently, Takeda et al. (2009) previously carried out an extensive spectroscopic investigation for 122 A-type stars (including 23 Am stars and 23 Hyades stars)⁵ covering a wide range of rotational velocities ($10 \lesssim v_e \sin i \lesssim 300 \text{ km s}^{-1}$). Although the main attention of that paper was paid to the Na I 5890/5896 lines of these stars, their abundances of O, Si, Ca, Ba, and Fe were also determined (cf. Table 1 in Takeda et al. 2009) by the spectrum fitting in the 6140–6170 Å region (similar to that we have done for IW Per; cf. Fig. 5), which makes us possible to discuss how IW Per is compared with other A-type stars in terms of the abundances of these Am-specific elements.

The behaviors of the $[X/H]$ values (abundances relative to the standard star Procyon which is known to have almost the solar composition, where X is any of O, Si, Ca, Ba, and Fe)⁶ for IW Per and 122 A-type stars are shown in Fig. 8, where their dependences upon T_{eff} and $v_e \sin i$ as well as mutual correlations are displayed. An inspection of Fig. 8 reveals the following trends.

- It is no doubt that IW Per is an Am star because the resulting abundances distinctly show characteristic trends of Am phenomena (e.g., underabundance in O and Ca, overabundance in Ba and Fe).

⁵By consulting the spectral types in three compilations (SIMBAD database, Bright Star Catalogue, and Hipparcos catalogue), those classified as “Am” in at least two out of these three sources were regarded as Am stars in this study: they are HD 20320, 23281, 27045, 27628, 27749, 28226, 28546, 29479, 29499, 30121, 30210, 33204, 33254, 33641, 40932, 48915, 72037, 95608, 141795, 173648, 198639, 204188, and 207098. Meanwhile, 23 Hyades stars are the same as indicated in Table 1 of Takeda et al. (2009).

⁶ $[X/H]_* \equiv A_* - A_{\text{procyon}}$, where A_{procyon} is 8.87 (O), 7.14 (Si), 6.19 (Ca), 2.33 (Ba), and 7.49 (Fe), which were determined from the 6140–6170 Å fitting in the similar manner (cf. the footnote in Sect. IVc of Takeda et al. 2008). IW Per have $[O/H] = -0.19$, $[Si/H] = +0.01$, $[Ca/H] = -0.29$, $[Ba/H] = +0.99$, and $[Fe/H] = +0.15$.

- However, answering the question about the degree of Am anomaly in IW Per is not so simple as it appears to differ from element to element. (i) Regarding O and Ca (which generally show deficiency in Am stars), the extent of peculiarity in this star is apparently less manifest as compared to slowly rotating Am stars (Figs. 8f and 8h). (ii) Meanwhile, the abundances of Si and Fe (both are correlated and tend to be enriched) in IW Per are not much different from those of other Am stars (Figs. 8g and 8j). (iii) Yet, it is remarkable that IW Per shows a conspicuous overabundance of Ba by as large as $\sim +1$ dex in spite of its being a rapid rotator (Fig. 8i).
- Therefore, while it is intuitively reasonable that O and Ca (deficiency group) show weaker peculiarity in IW Per (because rapid rotation near to the upper limit of Am phenomenon should have acted to suppress the anomaly), it is hard to understand why Ba (representative enrichment group) is so anomalously overabundant in the same star.
- These results suggest that the impact of rotation on the chemical anomaly is likely to act differently on each element in a complex way. Likewise, as to the issue of whether or not the abundance peculiarity in Am stars progressively declines with an increase in $v_e \sin i$, it is hard to give a simple answer, because some elements exhibit such a systematic trend (e.g., O, Ca) while others do not (e.g., Ba, showing rather a large dispersion).

8. Summary and conclusion

IW Per is a single-lined spectroscopic binary, which shows a slight periodic change in its brightness, since the orbital period is so short (0.92 d) that the stellar shape is distorted due to the centrifugal force (ellipsoidal variable).

This star is classified as belonging to the group of A-type metallic-line (Am) stars, which are often found in slow rotators as well as in close binary systems, and generally show anomalous line strengths of specific elements (e.g., O, Ca, Sc lines are weak, while lines of Fe-peak elements or s-process group are strong). It is noteworthy that IW Per is a rare Am star of rapid rotation ($v_e \simeq 100 \text{ km s}^{-1}$) near to the upper limit for the appearance of chemical peculiarity.

Previously, Kim (1980) reported based on his spectroscopic observations of IW Per that the equivalent widths of Ca II 3934, Sr II 4215, and Sc II 4320 lines (important lines characterizing the Am anomaly) show cyclic variations in accordance with the rotation phase. This is an important implication that chemical peculiarities on the surface of IW Per are not uniformly distributed but are rather patchy (an unusual case which is barely found in other Am stars). Unfortunately, this finding has acquired little attention and any follow-up study for its reconfirmation seems to have never been tried so far.

Motivated by this situation, 10 high-dispersion spectra of IW Per covering different phases were analyzed by applying the spectrum-fitting technique to the regions comprising these lines to determine the abundances of Ca, Sr, and Sc, from which the relevant equivalent widths (W_{3934} , W_{4215} , W_{4320}) were calculated. Likewise, in order to examine the characteristics of Am anomaly, the abundances of O, Si, Ca, Ba, and Fe were also established from the fitting analysis in the 6130–6180 Å region.

The resulting W data revealed no such clear phase-dependent variations as found by Kim (1980) (though some partly similar trend can not be excluded for W_{3934}). It is evident, however, W_{4215} as well as W_{4320} are essentially phase-independent and their fluctuations are reasonably explained by S/N-related uncertainties of the continuum level, which suggests that patchy abundance distributions of these elements are improbable.

Accordingly, contrary to the finding of Kim (1980), we conclude that any appreciable inhomogeneity of abundance anomaly on the surface of IW Per is unlikely, at least at the time of our observations in 2010 December. Although this consequence does not necessarily mean that Kim's (1980) result was incorrect (i.e., the situation might have changed with time), his measurements based on photographic spectrograms had better be viewed with caution.

In connection with searching for any variability in W , for that the local atmospheric parameters (T_{eff} and $\log g$) of an ellipsoidal variable such as IW Per weakly depend upon the position on the surface, its impact on the spectrum variation of a rotating star was also checked based on a model star of Roche potential surface. But this effect on the line strength was found to be insignificant (except for the Ca II 3934 line, which may suffer some change by this cause).

Finally, the abundances of O, Si, Ca, Ba, and Fe confirm that IW Per has typical abundance characteristics of Am stars (O and Ca are deficient; Ba and Fe are overabundant), despite that its rapid rotation is almost near to the upper limit of Am stars. Yet, it is not easy to answer the question whether the chemical anomaly in this rapidly rotating Am star is quantitatively less manifest as compared to other slower rotators, because the degree of peculiarity differs from element to element (e.g., while deficits in O and Ca are surely milder, excess in Ba is still considerably large).

Acknowledgements. This investigation has made use of the SIMBAD database, operated by CDS, Strasbourg, France, and the VALD database operated at Uppsala University, the Institute of Astronomy RAS in Moscow, and the University of Vienna.

REFERENCES

- Abt, H. A., & Morrell, N. I. 1995, *ApJS*, **99**, 135.
- Burkhart, C. 1979, *A&A*, **74**, 38.
- Cayrel, R. 1988, in *The Impact of Very High S/N Spectroscopy on Stellar Physics, Proceedings of IAU Symposium 132*, ed. G. Cayrel de Strobel, M. Spite (Kluwer, Dordrecht), p.345.
- Conti, P. S. 1970, *PASP*, **82**, 781.
- Gray, D. F. 2005, *The Observation and Analysis of Stellar Photospheres, Third Edition* (Cambridge University Press: Cambridge, UK).
- Hakkila, J., Myers, J. M., Stidham, B. J., & Hartmann, D. H. 1997, *AJ*, **114**, 2043.
- Kim, T.-H. 1980, *Ap&SS*, **68**, 355.
- Kodaira, K. 1975, in *Physics of Ap Stars, IAU Colloq. 32*, ed. W.W. Weiss, H. Jenkner, H.J. Wood (Universitätssternwarte Wien, Vienna), p.675.
- Kurucz, R. L. 1993, *Kurucz CD-ROM*, No. 13 (Harvard-Smithsonian Center for Astrophysics).
- Kurucz, R. L., & Bell, B. 1995, *Kurucz CD-ROM*, No. 23 (Harvard-Smithsonian Center for Astrophysics).
- Napiwotzki, R., Schönberner, D., & Wenske, V. 1993, *A&A*, **268**, 653.
- Paunzen, E. 2015, *A&A*, **580**, A23.
- Preston, G. W. 1974, *ARA&A*, **12**, 257.
- Ryabchikova, T., Piskunov, N., Kurucz, R. L., Stempels, H. C., Heiter, U., Pakhomov, Yu., & Barklem, P. S. 2015, *Phys. Scr.*, **90**, 054005.
- Takeda, Y. 1995, *PASJ*, **47**, 287.
- Takeda, Y., Han, I., Kang, D.-I., Lee, B.-C., & Kim, K.-M. 2008, *JKAS*, **41**, 83.
- Takeda, Y., Kang, D.-I., Han, I., Lee, B.-C., & Kim, K.-M. 2009, *PASJ*, **61**, 1165.
- Takeda, Y., & Sadakane, K. 1997, *PASJ*, **49**, 367.

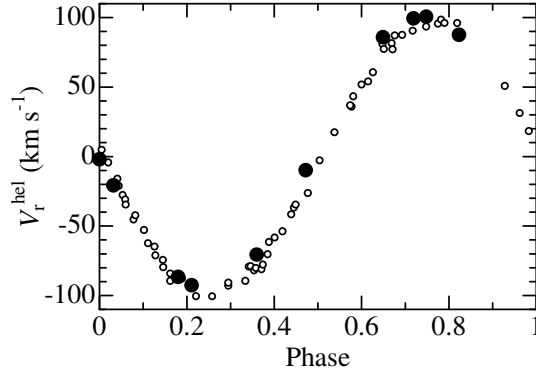


Fig. 1. Observed heliocentric radial velocities of IW Per (cf. Table 2) are plotted against the phase by larger filled symbols, while Kim's (1980) results are also overplotted by smaller open symbols for comparison.

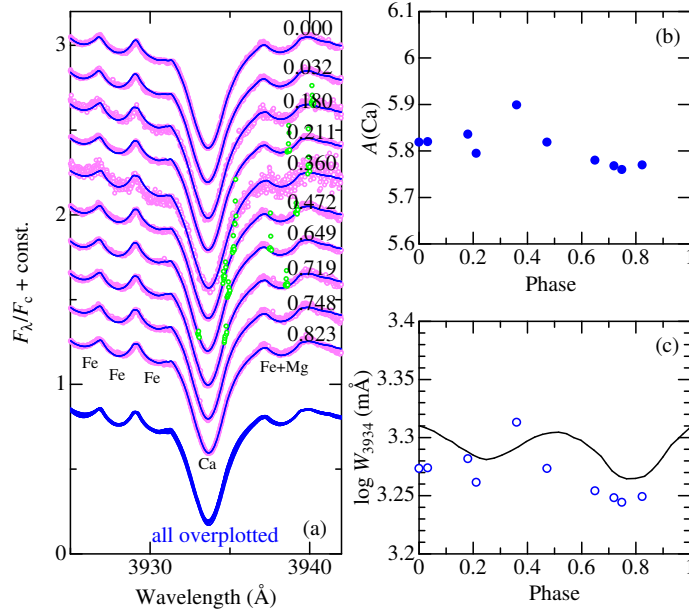


Fig. 2. (a) Synthetic spectrum fitting in the 3925–3942 Å region comprising the Ca II 3934 line. The observed 10 spectra at different phases (each shifted vertically relative to the adjacent one) are plotted in pink symbols (where the masked pixels are colored in light-green) while the best-fit theoretical spectra are shown in blue solid lines. The wavelength scale is adjusted to the laboratory system. In the bottom of the panel, all of these 10 theoretical spectra are overplotted (their residual flux scale is in the left ordinate) in order to show how they are compared with each other. (b) Ca abundances derived from this spectrum fitting (cf. Table 4) are plotted against the phase. (c) Equivalent widths of the Ca II 3934 line (cf. Table 4) are plotted against the phase, where the relation derived by Kim (1980; read from his Fig. 8) is also plotted by the solid line for comparison.

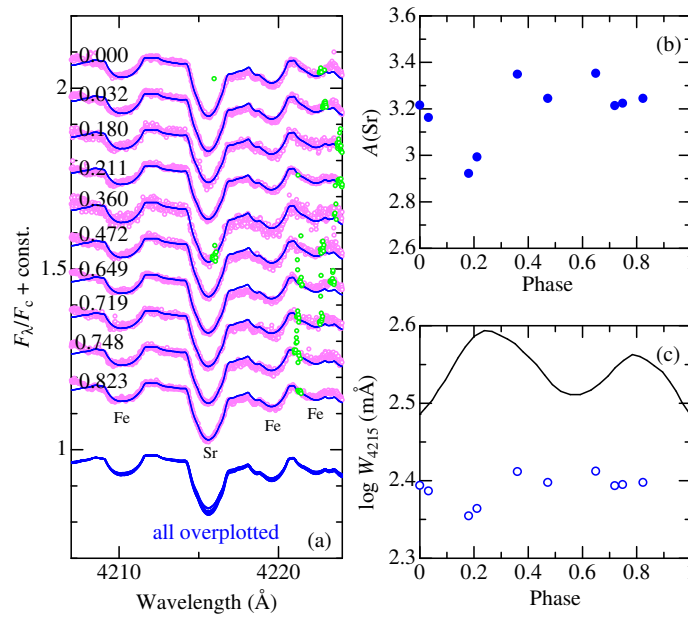


Fig. 3. (a) Synthetic spectrum fitting in the 4207–4224 Å region comprising the Sr II 4215 line. (b) Sr abundance vs. phase relation. (c) Sr II 4215 equivalent width vs. phase relation. Otherwise, the same as in Fig. 2.

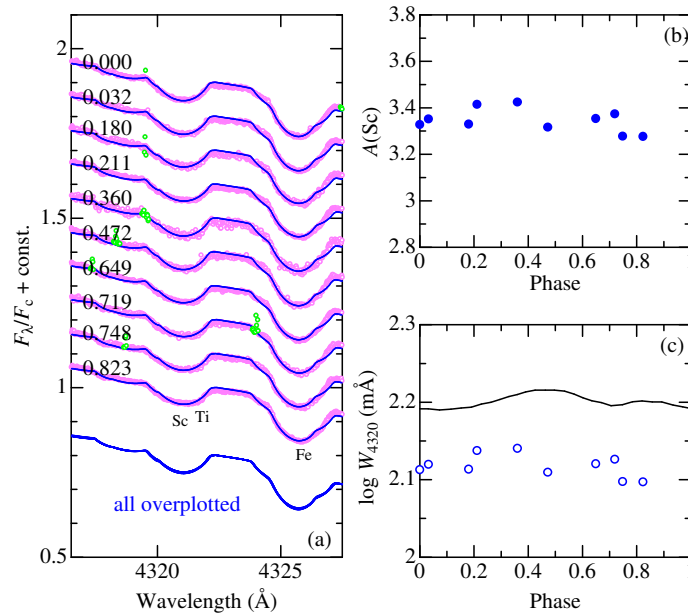


Fig. 4. (a) Synthetic spectrum fitting in the 4316.5–4327.5 Å region comprising the Sc II 4320 line. (b) Sc abundance vs. phase relation. (c) Sc II 4320 equivalent width vs. phase relation. Otherwise, the same as in Fig. 2.

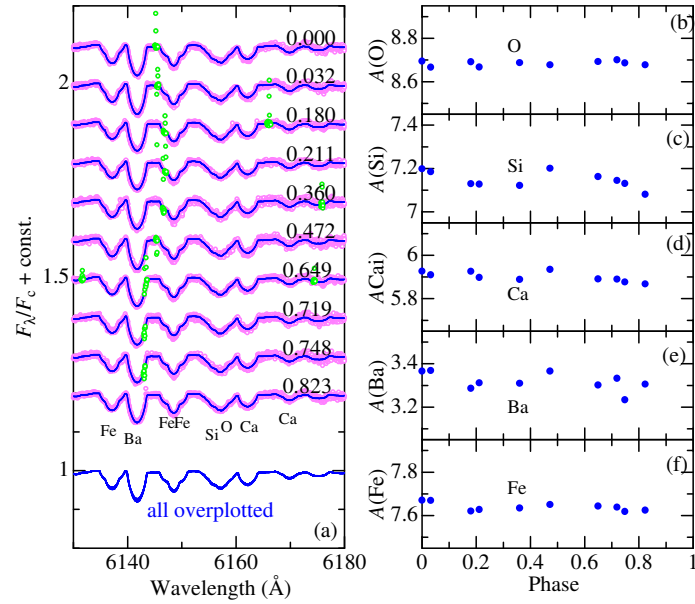


Fig. 5. (a) Synthetic spectrum fitting in the 6130–6180 \AA region comprising the lines of O, Si, Ca, Ba, and Fe. (b)–(f) The abundances of O, Si, Ca, Ba, and Fe derived from the fitting (cf. Table 4) are plotted against the phase. Otherwise, the same as in Fig. 2.

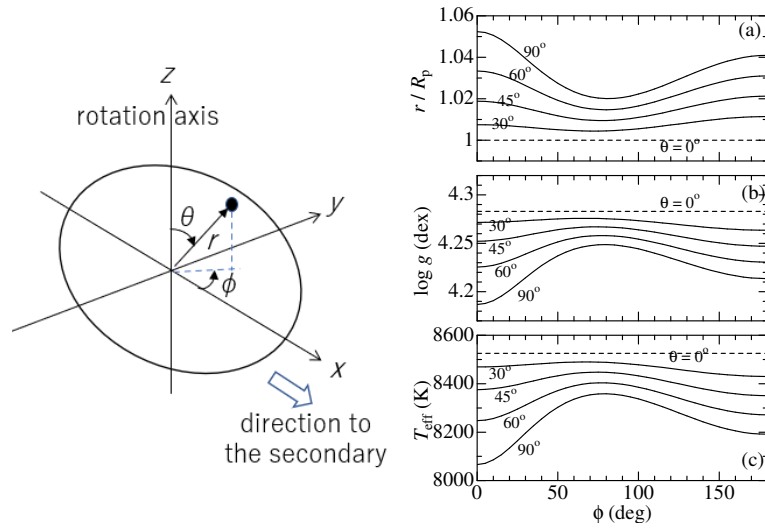


Fig. 6. Roche model calculated for the primary of IW Per. The parameters at the surface are expressed in the spherical coordinate system (r , θ , ϕ ; see the left-hand side of this figure for their definition). (a) Radius, (b) surface gravity, and (c) effective temperature.

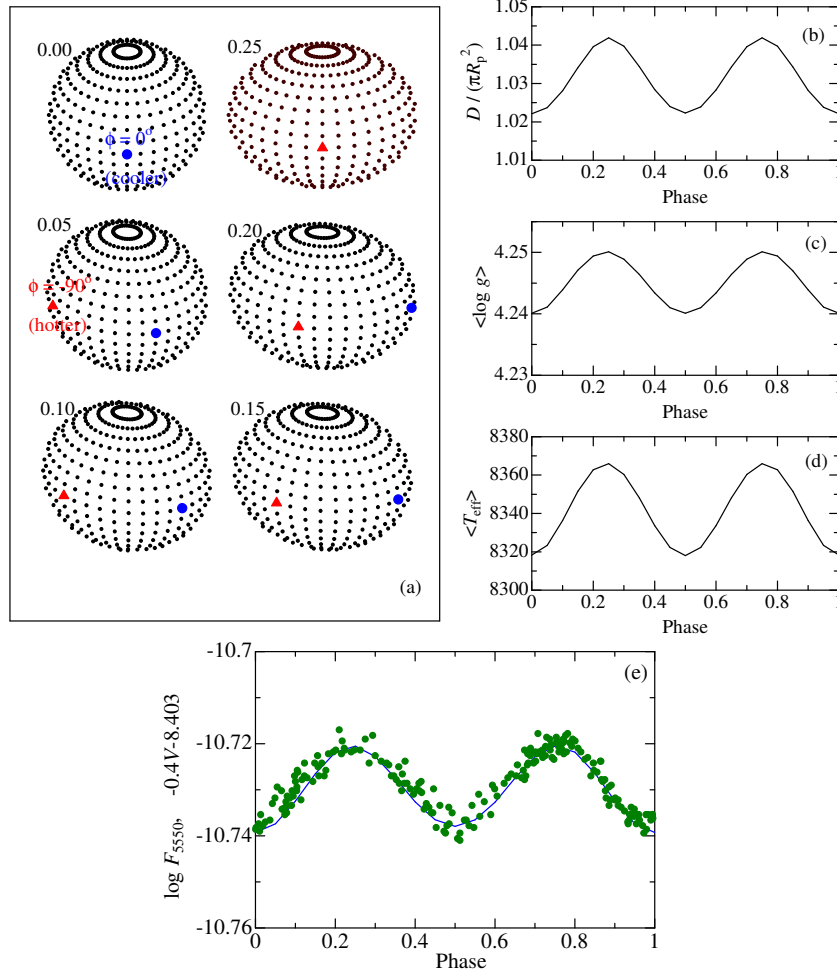


Fig. 7. (a) Schematic view of the primary of IW Per for six representative phases; 0.00, 0.05, 0.10, 0.15, 0.20, and 0.25, where the oblateness of star shape is purposely exaggerated. The $\phi = 0^\circ$ and $\phi = -90^\circ$ points at the equator ($\theta = 90^\circ$) are also indicated by filled circles and filled triangles, respectively. (b) Run of the visible disk area (D , in unit of πR_p^2) with phase. (c) Run of the disk-averaged surface gravity ($\langle \log g \rangle$) with phase. (d) Run of the disk-averaged effective temperature ($\langle T_{\text{eff}} \rangle$) with phase. (e) The run of F_{5550} (theoretical flux at 5550 \AA at the earth in unit of $\text{erg cm}^{-2} \text{ s}^{-1} \text{ \AA}^{-1}$, which is calculated by disk integration) with phase is shown by the solid line. The observed fluxes corresponding to the V magnitudes of IW Per (derived from the ΔV data given in Table IVa of Kim 1980 along with his comparison star magnitude of $V = 6.52$) are also depicted by symbols (cf. Sect. 5 for the explanation on the offset constant of -8.403).

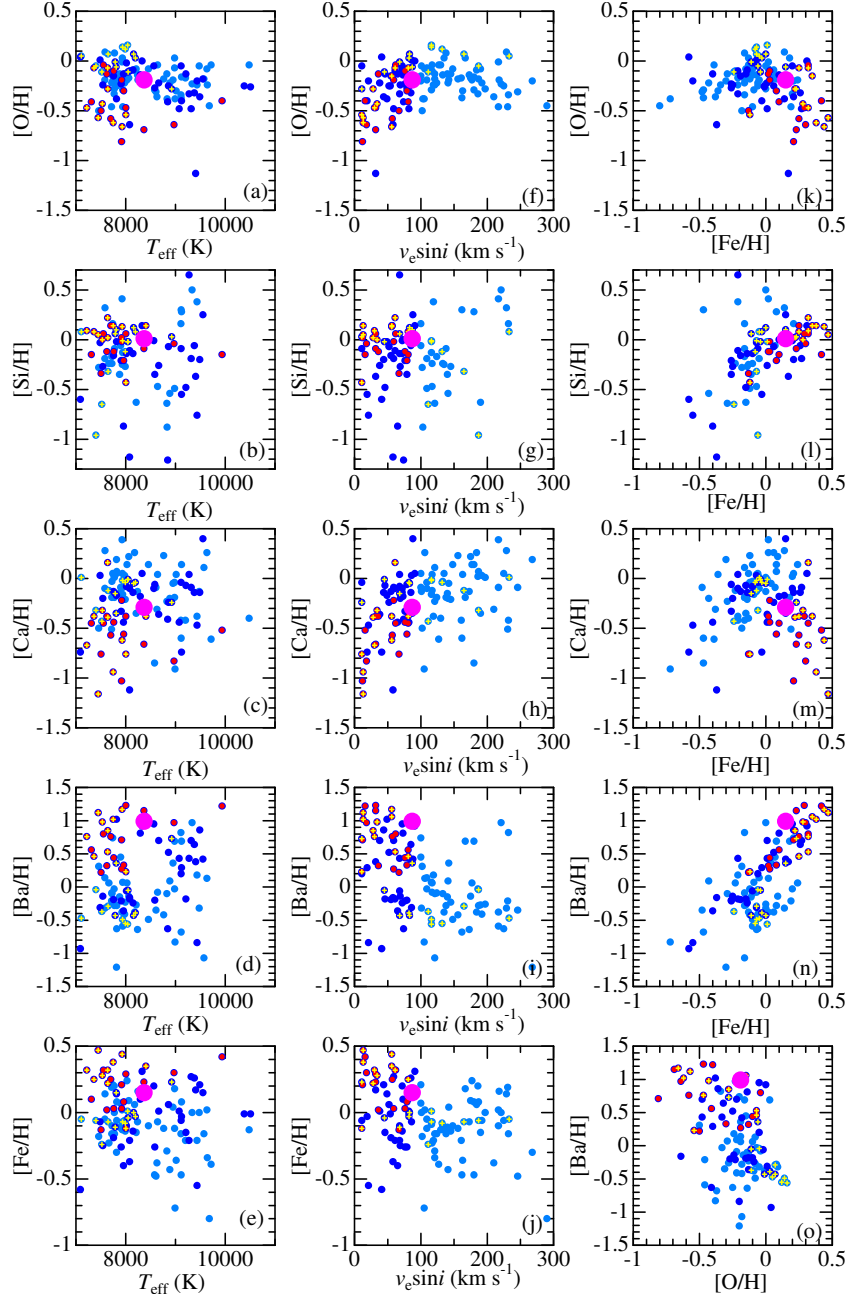


Fig. 8. Graphical display showing the characteristics of $[O/H]$, $[Si/H]$, $[Ca/H]$, $[Ba/H]$, and $[Fe/H]$ derived for IW Per from the 6130–6180 Å fitting (differential abundances of O, Si, Ca, Ba, and Fe relative to the standard star Procyon; practically the same composition as the Sun) in comparison with those of 122 A-type stars previously determined by Takeda et al. (2009), where the data for IW Per are highlighted by pink large symbols. These $[O/H]$, $[Si/H]$, $[Ca/H]$, $[Ba/H]$, and $[Fe/H]$ values are plotted against T_{eff} in the left panels (a–e) and against $v_e \sin i$ in the center panels (f–j). In the right panels (k–o) are shown the mutual correlations between these abundances: $[X/H]$ values ($X = O, Si, Ca, Ba$) are plotted against $[Fe/H]$ in panels (k–n), while the right-bottom panel (o) displays the $[Ba/H]$ vs. $[O/H]$ diagram. Regarding 122 A-type stars, those of lower $v_e \sin i$ ($< 100 \text{ km s}^{-1}$) and higher $v_e \sin i$ ($\geq 100 \text{ km s}^{-1}$) are discriminated in dark blue and light blue, respectively. Also, those 23 stars classified as Am are distinguished by overplotting small red-filled circles, while yellow crosses are overplotted for 23 Hyades cluster stars.

Table 1: Orbital and stellar parameters of IW Per adopted in this study

Parameter	Value	Unit	Explanation
[Orbital and stellar parameters taken from Kim (1980)]			
P	0.9171877	day	orbital period
T_0	2433617.317	Julian Day	Origin of light minimum (phase = 0)
K	99.3	km s ⁻¹	Radial velocity amplitude
γ	0.2	km s ⁻¹	system radial velocity
e	0.02	...	ellipticity
ω	106.9	deg	longitude of periastron
i	63	deg	inclination angle
M_1	2.0	M_\odot	mass of the primary
M_2	1.08	M_\odot	mass of the secondary
R_1	1.7	R_\odot	radius of the primary ($\equiv R_p$; polar radius)
R_2	1.0	R_\odot	radius of the secondary
a_1	2.03	R_\odot	distance between the primary and the center of gravity
a_2	3.76	R_\odot	distance between the secondary and the center of gravity
s_{12}	5.79	R_\odot	separation between the primary and the secondary
[Colors and atmospheric parameters]			
* $b - y$	0.057	mag	Strömgren's $b - y$ color
* m_1	0.229	mag	Strömgren's m_1 index
* c_1	0.945	mag	Strömgren's c_1 index
* β	2.880	mag	Strömgren's β index
† T_{eff}	8371	K	effective temperature
† $\log g$	4.22	dex	logarithmic surface gravity (in c.g.s.)
# v_t	3.89	km s ⁻¹	microturbulence

* Taken from Paunzen (2015).

† Derived from colors of the Strömgren system by using Napiwotzki et al.'s (1993) UVBYBETANEW program.

Derived from Takeda et al.'s (2008) T_{eff} -dependent empirical relation

Table 2: Basic information of the observational spectra

Sp.code	N_f	Exp.T	HJD	Phase	V_r^{hel}	SN ₃₉₃₄	SN ₄₂₁₅	SN ₄₃₂₀	SN ₆₁₅₀
(1)	(2)	(3)	(4)	(5)	(6)	(7)	(8)	(9)	(10)
1218B	2	35	2455549.110	0.000	-2.0	130	300	300	350
1220A	1	15	2455550.973	0.032	-20.7	170	280	290	350
1218C	1	20	2455549.274	0.180	-86.6	80	170	230	350
1220B	2	30	2455551.138	0.211	-92.6	160	330	370	360
1220C	1	20	2455551.274	0.360	-70.6	30	110	140	250
1214A	2	40	2455544.956	0.472	-9.9	100	210	230	240
1216A	2	30	2455546.953	0.649	+85.8	160	280	340	380
1214B	2	40	2455545.183	0.719	+99.4	120	220	260	280
1215A	2	40	2455546.126	0.748	+100.6	130	220	260	290
1218A	2	30	2455548.947	0.823	+87.6	200	340	430	390

(1) Spectrum code. For example, “1218B” denotes the second [B] observation on 2010 December 18 [1218], or “1216A” corresponds to the first [A] observation on 2010 December 16 [1216]. (2) Number of frames co-added to obtain the final spectrum. (3) Total exposure time (in unit of min). (4) Heliocentric Julian Day at the time of mid-exposure. (5) Orbital phase calculated by Eq. (1). (6) Heliocentric radial velocity (in unit of km s⁻¹) determined by the spectrum fitting in the 6130–6180 Å region. (7) Mean S/N ratio around the Ca II 3934 line. (8) Mean S/N ratio around the Sr II 4215 line. (9) Mean S/N ratio around the Sc II 4320 line. (10) Mean S/N ratio in the 6130–6180 Å region.

Note that these data are arranged in the ascending order of the orbital phase.

Table 3: Atomic data of important lines.

Species	λ	χ_{low}	$\log gf$	Species	λ	χ_{low}	$\log gf$
Ca II	3933.664	0.000	+0.105	O I	6155.989	10.740	-1.161
Sr II	4215.519	0.000	+0.145	O I	6156.737	10.740	-1.521
Sc II	4320.732	0.605	-0.260	O I	6156.755	10.740	-0.931
Fe I	6137.694	2.588	-1.403	O I	6156.778	10.740	-0.731
Ba II	6142.928	0.552	-0.992	O I	6158.149	10.741	-1.891
Si I	6143.125	5.964	-2.790	O I	6158.172	10.741	-1.031
Si I	6145.016	5.616	-0.820	O I	6158.187	10.741	-0.441
Fe II	6147.741	3.889	-2.721	Ca I	6161.297	2.523	-1.020
Fe II	6149.258	3.889	-2.724	Ca I	6162.173	1.899	+0.100
Fe I	6151.617	2.176	-3.299	Ca I	6163.755	2.521	-1.020
Si I	6155.134	5.619	-0.400	Fe I	6165.361	4.143	-1.550
O I	6155.961	10.740	-1.401	Ca I	6166.439	2.521	-0.900
O I	6155.971	10.740	-1.051				

Given are the species, air wavelength (in Å), lower excitation potential (in eV), and logarithm of statistical weight (of the lower level) times absorption oscillator strength (in dex).

Table 4: Resulting abundances and corresponding equivalent widths.

Sp.code	Phase	$A(\text{Ca})$ (dex)	W_{3934} (mÅ)	$A(\text{Sr})$ (dex)	W_{4215} (mÅ)	$A(\text{Sc})$ (dex)	W_{4320} (mÅ)	$A(\text{O})$ (dex)	$A(\text{Si})$ (dex)	$A(\text{Ca})$ (dex)	$A(\text{Ba})$ (dex)	$A(\text{Fe})$ (dex)	$v_e \sin i$ (km s ⁻¹)
		[Ca II 3934]		[Sr II 4215]		[Sc II 4320]		[Solutions from the 6130–6180 Å region fitting]					
1218B	0.000	5.82	1877	3.22	248	3.33	130	8.70	7.20	5.93	3.37	7.67	85.2
1220A	0.032	5.82	1879	3.16	244	3.35	132	8.67	7.19	5.91	3.37	7.67	85.2
1218C	0.180	5.84	1914	2.92	226	3.33	130	8.69	7.13	5.93	3.29	7.62	87.7
1220B	0.211	5.80	1826	2.99	231	3.42	137	8.67	7.13	5.90	3.31	7.63	88.7
1220C	0.360	5.90	2057	3.35	258	3.43	138	8.69	7.12	5.89	3.31	7.64	87.0
1214A	0.472	5.82	1877	3.25	250	3.32	129	8.68	7.20	5.94	3.37	7.65	85.1
1216A	0.649	5.78	1795	3.35	258	3.35	132	8.69	7.16	5.89	3.30	7.64	87.2
1214B	0.719	5.77	1771	3.21	248	3.37	134	8.70	7.15	5.89	3.33	7.64	89.2
1215A	0.748	5.76	1755	3.22	248	3.28	125	8.69	7.13	5.88	3.23	7.62	87.4
1218A	0.823	5.77	1775	3.25	250	3.28	125	8.68	7.08	5.87	3.31	7.63	86.3
	(mean)	5.81	1853	3.19	246	3.35	131	8.68	7.15	5.90	3.32	7.64	86.9
	(std.dev.)	0.04	90	0.14	10	0.05	4	0.01	0.04	0.02	0.04	0.02	1.4

Given are the abundances (A) derived from the spectrum fitting analysis in each of the 4 regions, and the corresponding equivalent widths (W) of Ca II 3934, Sr II 4215, and Sc II 4320 lines inversely derived from the abundance solutions. The mean values and their standard deviations are also presented in the last two rows. As usual, $A(X)$ is the logarithmic number abundance of element X normalized with respect to H as $A(\text{H}) = 12.00$.

Table 5: Variations of equivalent widths in response to changing T_{eff} or $\log g$.

Line	A_{given}	W_{std}	W_{T+}	W_{T-}	W_{g+}	W_{g-}	δ_{T+}	δ_{T-}	δ_{g+}	δ_{g-}
Ca II 3934	5.807	1851.6	1527.2	2231.2	1855.5	1848.7	-0.175	+0.205	+0.002	-0.002
Sr II 4215	3.192	245.9	229.0	261.9	245.6	246.2	-0.069	+0.065	-0.001	+0.001
Sc II 4320	3.345	131.2	117.7	143.4	129.9	132.6	-0.103	+0.093	-0.010	+0.011

Given in columns 3–7 are the equivalent widths in mÅ (for the given abundance A_{give} , which is the mean of the 10 A values for different phases; cf. Table 4) calculated for the standard model atmosphere ($T_{\text{eff}} = 8371$ K, $\log g = 4.22$) and four model atmospheres in which T_{eff} or $\log g$ is interchangeably varied from the standard values (suffixes ‘ $T+$ ’, ‘ $T-$ ’, ‘ $g+$ ’, and ‘ $g-$ ’ denote the cases of $\Delta T_{\text{eff}} = +250$ K, $\Delta T_{\text{eff}} = -250$ K, $\Delta \log g = +0.05$, and $\Delta \log g = -0.05$, respectively). The relative changes of W are also presented in the following columns 8–11 ($\delta_{T+} \equiv (W_{T+} - W_{\text{std}})/W_{\text{std}}$, etc.).